**The Cryosphere
Discussions**

A general treatment of snow microstructure exemplified by an improved relation for the thermal conductivity

H. Löwe, F. Riche, and M. Schneebeli

WSL Institute for Snow and Avalanche Research SLF, Davos, Switzerland

Correspondence to: H. Löwe (loewe@slf.ch)

Title Page

Abstract	Introduction
Conclusions	References
Tables	Figures

|◄ | ►|
◄ | ►

Back | Close

Full Screen / Esc

Printer-friendly Version

Interactive Discussion

A general treatment of snow microstructure

H. Löwe et al.

Abstract

Finding relevant microstructural parameters beyond the density is a longstanding problem which hinders the formulation of accurate parametrizations of physical properties of snow. Towards a remedy we address the effective thermal conductivity tensor of snow via known anisotropic, second-order bounds. The bound provides an explicit expression for the thermal conductivity and predicts the relevance of a microstructural anisotropy parameter Q which is given by an integral over the two-point correlation function and unambiguously defined for arbitrary snow structures. For validation we compiled a comprehensive data set of 167 snow samples. The set comprises individual samples of various snow types and entire time series of metamorphism experiments under isothermal and temperature gradient conditions. All samples were digitally reconstructed by micro-computed tomography to perform microstructure-based simulations of heat transport. The incorporation of anisotropy via Q considerably reduces the root mean square error over the usual density-based parametrization. The systematic quantification of anisotropy via the two-point correlation function suggests a generalizable route to incorporate microstructure into snowpack models. We indicate the inter-relation of the conductivity to other properties and outline a potential impact of Q on dielectric constant, permeability and adsorption rate of diffusing species in the pore space.

1 Introduction

The inter-relation between different physical properties of snow and their microstructural origin is crucial for a broad range of cryospheric applications, e.g. thermal conductivity and dielectric properties for microwave signatures (Barber and Nghiem, 1999), thermal conductivity and air permeability for mega-dune formation (Courville et al., 2007) or thermal conductivity and shear-strength for field characterization (Domine et al., 2011). Snow microstructure plays also a key role for natural hazards (Schweizer

Full Screen / Esc

et al., 2003) or aspects of climate sensitivity (Fichefet et al., 2000; Flanner and Zender, 2006).

Snow properties are usually parametrized phenomenologically. The ice volume fraction ϕ_i (density) is the most important microstructural quantity which correlates well with physical properties. However, a large scatter remains if properties are constrained on density as, e.g. revealed for the thermal conductivity in Sturm et al. (1997); Domine et al. (2012). This scatter was recently investigated by simulations and experiments in a comprehensive study by Calonne et al. (2011). The authors hypothesized that the remaining scatter in the thermal conductivity is caused by microstructural anisotropy. As we shall show below, anisotropy has in fact a severe impact on thermal conductivity and can be utilized quantitatively, if formalized by appropriate means.

In the last three decades powerful theoretical concepts have been developed for heterogeneous materials (Torquato, 2002). In particular, series expansions yield formally exact expressions for various physical properties. Relevant for snow are so called strong-contrast expansions which are available for the thermal or electrical conductivity (Sen and Torquato, 1989), elasticity (Torquato, 1997) and complex dielectric tensor (Rechtsman and Torquato, 2008). The expansion parameter is a rational function of the phase properties and the expansion coefficients can be computed explicitly in terms of n-th order correlation functions. In other words, series expansions provide explicit expressions for the physical properties in terms of a complete, hierarchical sequence of microstructural parameters with increasing complexity. The advantage of these series are their good convergence properties over a large range of volume fractions, even for strong contrast, i.e. strongly different phase properties. This is well suited for snow where ice and air properties usually differ by an order of magnitude. Truncations of series expansions at a certain order lead to approximations for the physical properties, which can be recast into rigorous bounds, e.g. for the conductivity (Torquato and Sen, 1990). For isotropic materials the second-order bounds only involve the volume fraction (Ch. 21, Torquato, 2002) and could thus not be used to address the aforementioned scatter at fixed density. Second-order bounds for anisotropic materials however

include, besides the volume fraction, an additional microstructural anisotropy parameter Q (Torquato and Sen, 1990).

In this paper we adapt this approach to snow and demonstrate the relevance of the parameter Q which can be formally regarded as a depolarization factor for a random arrangement of aligned (hard or overlapping) spheroids (Torquato and Lado, 1991). The treatment of anisotropy is however very different from the granular viewpoint (Shertzer and Adams, 2011) based on grain contacts which are difficult to define. Similar to previous work (Kaempfer et al., 2005; Calonne et al., 2011; Riche and Schneebeli, 2012) we employ microstructure based simulations on tomography image data and restrict ourselves to purely conductive heat transport. In addition, the present approach yields an accurate model for the thermal conductivity which can be unambiguously evaluated from the geometry of the ice matrix. The method is not restricted to the thermal conductivity as we outline in the discussion. We believe that our results constitute an essential step towards a unified macroscopic modeling of snow which will certainly benefit from incorporating anisotropy within a formulation of metamorphism in terms of correlation functions.

2 Theory

2.1 Two point correlation function

Like any two-phase material, snow can be fully characterized at the pore level by a phase indicator function $\phi_i(r)$ which is unity if $r \in \mathbb{R}^3$ is in the ice phase and zero otherwise. For the present purpose we need the first and second-order correlators of ϕ_i, namely the volume fraction $\phi_i = \overline{\phi_i(r)}$ and the two-point correlation function

$$C(r) = \overline{\phi_i(x+r)\phi_i(x)} - \phi_i^2 \tag{1}$$

where volume averaging is denoted by $\overline{\bullet}$.

2.2 Anisotropic second order bound

Sen and Torquato (1989) derived an exact series expansion of the effective conductivity tensor k_e for anisotropic materials of arbitrary microstructure. This expansion was used by Torquato and Sen (1990) to derive upper and lower bounds for k_e. To apply the
5 bound it is convenient to make a simplifying assumption about the structure of snow in the first place. We assume transverse isotropy in xy plane. This is reasonable for snowpacks in which temperature gradients are usually aligned in z direction. Then the two-point correlation function $C(r) = C(r, \cos\theta)$ solely depends on the magnitude $r = |r|$ and the polar angle θ relative to the z-axis, viz. $\cos\theta = r \cdot e_z$. Under these assumptions
10 the effective conductivity tensor k_e is diagonal and the diagonal entries are bounded from below by (Torquato and Sen, 1990)

$$k_{e,x}^{(L)} = k_{e,y}^{(L)} = k_{air}\frac{1 + [\phi_i + (1 - \phi_i)Q](\alpha - 1)}{1 + (1 - \phi_i)Q(\alpha - 1)} \tag{2}$$

$$k_{e,z}^{(L)} = k_{air}\frac{1 + [\phi_i + (1 - \phi_i)(1 - 2Q)](\alpha - 1)}{1 + (1 - \phi_i)(1 - 2Q)(\alpha - 1)} \; .$$

15 Here $\alpha = k_{ice}/k_{air}$ denotes the ratio of the phase conductivities of ice and air which is typically in the order of 100. The microstructural parameter Q in Eq. (2) is defined by an integral over the two-point correlation function,

$$Q = \frac{1}{3} - \lim_{\delta \to 0} \frac{1}{2\,\phi_i(1 - \phi_i)} \int_{\delta}^{\infty} \frac{dr}{r} \int_{0}^{\pi} d(\cos\theta)P_2(\cos\theta)C(r) \tag{3}$$

where $P_2(x) = (3x^2 - 1)/2$ denotes the Legendre polynomial of order two. In the
20 isotropic case $C(r)$ is independent of θ and the integral in Eq. (3) vanishes, viz. $Q = 1/3$. The bound (Eq. 2) provides an approximation for the conductivity tensor in terms of the correlation function (Eq. 1) which can be computed for any microstructure.

The associated upper bound (Torquato and Sen, 1990) diverges for large α and is not further considered here.

2.3 Simplification of the bound for snow

Equation (3) is a Cauchy principal-value integral and the limit $\delta \to 0$ must be taken after integration. This is elaborate to carry out via direct numerical integration of Eq. (3) on 3-D image data. We prefer to assume an anisotropic functional form for C and compute the integral analytically. We have shown in (Löwe et al., 2011) that the anisotropic behavior of the two-point correlation function even in the absence of a temperature gradient turns out to be complex and cannot be described by a single length scale. In contrast in microwave modeling it is common to approximate the correlation function e.g. by a simple exponential form and a single correlation length (Vallese and Kong, 1981; Wiesmann et al., 1998). In the absence of available results for the correlation function for other than isothermal conditions we follow the simplification adopted in microwave modeling and focus on a single length scale.

To account for anisotropy we employ a spheroidal scaling form $C(r/l(\cos\theta))$ with a direction dependent correlation length $l(\cos\theta) = l_{xy}/[1-(1-(l_{xy}/l_z)^2)\cos^2\theta]^{1/2}$. Here l_z denotes the vertical and l_{xy} the horizontal correlation length, respectively. Denoting the ratio of correlation lengths by $\epsilon = l_z/l_{xy}$ we can directly re-use the algebra in (Torquato and Lado, 1991) to evaluate the integral in Eq. (3) and obtain

$$Q = \begin{cases} \dfrac{1}{2}\left\{1 + \dfrac{1}{\epsilon^2-1}\left[1 - \dfrac{1}{2\chi_b(\epsilon)}\ln\left(\dfrac{1+\chi_b(\epsilon)}{1-\chi_b(\epsilon)}\right)\right]\right\}, & \epsilon > 1, \\[2ex] \dfrac{1}{2}\left\{1 + \dfrac{1}{\epsilon^2-1}\left[1 - \dfrac{1}{\chi_a(\epsilon)}\mathrm{atan}(\chi_a(\epsilon))\right]\right\}, & \epsilon < 1. \end{cases} \tag{4}$$

with $\chi_a(\epsilon)^2 = -\chi_b(\epsilon)^2 = 1/\epsilon^2 - 1$. Both expressions in Eq. (4) yield $Q = 1/3$ for $\epsilon \to 1$. Together with Eq. (2) this constitutes our explicit expression for the effective conductivity.

3 Materials and methods

3.1 Snow samples

To provide a comprehensive data set for validation we compiled a heterogeneous collection of 167 snow samples. All samples were scanned with X-ray tomography (μCT) without casting procedures. We have analyzed two time series of isothermal experiments (denoted by ISO-1, ISO-5 henceforth) four time series of temperature gradient metamorphism experiments (TGM-2, TGM-17, DH-1, DH-2) and a set of 37 individual samples (DIV) comprising various types of snow. ISO-1 and ISO-5 are described in Löwe et al. (2011), TGM-17 is taken from Kaempfer et al. (2005), TGM-2 is measured in the snow-breeder (Pinzer and Schneebeli, 2009), DH-1, DH-2 are taken from Riche et al. (2012). A detailed characterization including the IACS international classification of seasonal snow on the ground (Fierz et al., 2009) of the snow samples is given in the Supplement. In summary we analyzed 62 depth hoars (DH), 54 rounded grains (RG), 33 faceted crystals (FC) 10 decomposing and fragmented precipitation particles (DF), 5 melt forms (MF) and 3 precipitation particles (PP).

3.2 Two-point correlation function and bound

To calculate the the two-point correlation function $C(\boldsymbol{r})$ from segmented tomography images we used Fast Fourier transformation to compute the convolution in Eq. (1). By fitting the correlation function along the coordinate axes $\beta = x, y, z$ to an exponential $C_\beta(r) = C_{\beta,0} \exp(-r/l_\beta)$, we obtained the correlation lengths $l_z, l_{xy} = (l_x + l_y)/2$ and the aspect ratio $\epsilon = l_z/l_{xy}$. The ratio ϵ was used to compute Q from Eq. (4) and eventually the bound from Eq. (2).

3.3 Finite element simulations

To simulate the thermal conductivity tensor $\boldsymbol{k}_e$ we have used a parallel version of a finite element code (Garboczi, 1998) which solves the variational formulation of the conductivity problem with periodic boundary conditions to minimize finite-size effects.

To incorporate the effect of temperature raised by Calonne et al. (2011) we adopted the scaling form $\boldsymbol{k}_e(k_{ice}, k_{air}) = k_{air}\boldsymbol{k}_e(k_{ice}/k_{air}, 1)$ (Ch. 13.2.5, Torquato, 2002). Thus the effective conductivity tensor depends only on the ratio $\alpha = k_{ice}/k_{air}$ of the phase conductivities. For temperatures $-20\,°C < T < 0\,°C$ the ratio varies roughly in the interval $90 < \alpha < 110$. By simulating $\boldsymbol{k}_e$ for three ice conductivities $k_{ice} = 2.107, 2.34, 2.6\,WK^{-1}\,m^{-1}$ at fixed air conductivity $k_{air} = 0.024\,WK^{-1}\,m^{-1}$ we obtain $\alpha = k_{ice}/k_{air} = 87.8, 97.3, 108.3$ which covers the relevant temperature range.

4 Results

4.1 Vertical conductivity vs. density

The simulated vertical conductivity $k_{e,z}$ ($k_{ice} = 2.107$, $k_{ice} = 0.024$) is shown in Fig. 1 as a function of volume fraction. We follow Calonne et al. (2011); Sturm et al. (1997) and fitted the data to a second order polynomial of the form $k_{e,z} = k_{air} + a\phi_i + b\phi_i^2$. The fit (solid black line) yields a root mean square error $\sigma = 0.32\,Wm^{-1}K^{-1}$. The inset shows the directionally averaged conductivity for comparison, where the black line is the respective least squares fit ($\sigma = 0.16\,Wm^{-1}K^{-1}$) and the red line is the fit obtained in Calonne et al. (2011) for the same values of k_{ice} and k_{air}. Note that Calonne et al. (2011) includes fewer depth hoar samples so a systematic difference between the fits is expected.

4.2 Vertical conductivity vs. bound

Next we compared the simulated vertical conductivity $k_{e,z}$ with the prediction of the bound $k_{e,z}^{(L)}$ from Eq. (2). For all values of $\alpha = k_{ice}/k_{air}$ we find a linear relation between simulations and the bound with $\sigma = 0.18\,\mathrm{W\,m^{-1}\,K^{-1}}$ independent of α. We can thus employ a simple linear correction to obtain the parametrization

$$k_{e,z} = k_{air}\left[A(\alpha)\,k_{e,z}^{(L)}/k_{air} - B(\alpha)\right]. \tag{5}$$

A comparison between simulated values for $k_{ice} = 2.34$, $k_{ice} = 0.024$ and Eq. (5) is shown in Fig. 2. The coefficients $A(\alpha) = 0.066\alpha + 0.871$ and $B(\alpha) = 0.084\alpha - 0.872$ can be well described by linear functions as shown in the inset in Fig. 2. To further illustrate the impact of Q, we compare Eq. (5) with the simulations for an individual time series (TGM-17) as shown in Fig. 3. In the inset we have plotted the time evolution of the two dimensionless parameters ϕ_i, Q during the experiment. This reveals that high frequency modulations in the evolution of $k_{e,z}$ stem from fluctuations in ϕ_i while the slow, non-monotonous modulation in $k_{e,z}$ originates from the evolution of Q. The distribution of the relevant microstructure parameters in the (ϕ_i, Q) plane is shown in Fig. 4.

4.3 Horizontal conductivity vs. bound

Finally we fit the horizontal conductivity $k_{e,xy}$ linearly to the bound $k_{e,xy}^{(L)}$ and obtain the behavior shown in Fig. 5. In contrast to the vertical case, the coefficients $A(\alpha), B(\alpha)$ are strikingly different and do not vary linearly with α.

5 Discussion

5.1 Improvement of microstructural characterization

Anisotropy and scatter are concealed if the conductivity is directionally averaged (inset Fig. 1). However, thermal fluxes in snowpacks are mostly governed by the vertical conductivity $k_{e,z}$. The scatter of vertical conductivity (Fig. 2) is reduced compared to a purely density based formulation (Fig. 1) by incorporating the microstructural parameter Q. It is not surprising that the bound must be corrected in magnitude via $A(\alpha)$ in Eq. (5); second-order bounds are generally known to be not very tight (Torquato, 2002). However, a key finding is the "linear" relation between the bound and simulations. This implies that the interplay between density and anisotropy is well reproduced by the functional form in Eq. (2). This is confirmed by Fig. 3 which discerns the impact of ϕ_i and Q on the overall evolution of the conductivity $k_{e,z}$ for a temperature gradient experiment. The non-monotonous evolution of $k_{e,z}(t)$ stems from the non-monotonous evolution of anisotropy $Q(t)$ which is only slightly modulated by fluctuations in the density. The increase in conductivity is generally attributed literally to chain-like or columnar structural features (Arons and Colbeck, 1995) while a decrease might again occur in the depth hoar regime (Sturm et al., 2002a). At the same time only minor changes in the density are observed which is the origin of stated limitations of density-based parametrizations (Sturm and Johnson, 1992; Sturm et al., 2002a; Domine et al., 2012). This is confirmed in Fig. 4 where Q evolves almost orthogonally to ϕ_i for temperature gradient experiments. Our results suggest that the anisotropy parameter Q well embodies what has been termed "metamorphic component" in Sturm et al. (2002b) to empirically constrain the conductivity of snow on sea ice for gradient-dominated snowpack conditions.

We do not observe apparent outliers, neither for isothermal metamorphism nor for other snow types (Fig. 2). The identification of a relevant parameter Q, which is unambiguously defined for arbitrary snow structures in terms of the correlation function $C(\mathbf{r})$, considerably simplifies the remaining task of investigating the evolution of Q or $C(\mathbf{r})$

during crystal growth under various metamorphism conditions. It seems thus feasible to include these effects into snowpack models required e.g. to assess the sensitivity of sea ice on snow conductivity (Fichefet et al., 2000). Besides the conductivity, we expect Q also to be relevant for other physical properties of snow as we indicate now.

5.2 Implication on other snow properties

Inferring the relevance of anisotropy for other properties is facilitated by mathematical similarities between the thermal conductivity and the dielectric tensor, diffusion of reactive tracers and fluid permeability (Sen and Torquato, 1989; Torquato, 2002). For the effective dielectric tensor ε_e of anisotropic materials we resort to the long wavelength approximation (Rechtsman and Torquato, 2008), applicable to microwave scattering. Their treatment is completely analogous to (Sen and Torquato, 1989) employed here for the conductivity. The second-order approximation (Eq. C.2, Rechtsman and Torquato, 2008) reveals that the z component of the dielectric tensor can be written in terms of Q. However, the phase contrast in the dielectric case $\alpha = \varepsilon_{ice}/\varepsilon_{air} \approx 3$ is significantly lower compared to the thermal case $\alpha \approx 100$. Specifically for $\alpha \approx 1$ the influence of anisotropy vanishes as correctly reflected by Eq. (2). We thus expect only a minor influence of anisotropy on the dielectric tensor.

Next we comment on the so called trapping constant γ (Torquato, 2002) which specifies the rate at which reactive species diffusing in the pore space get adsorbed on the ice interface. Using Eqs. (3.1)–(4), (2.40), (4.14)–(15) of Torquato and Lado (1991) we infer that the second-order anisotropic lower bound $\gamma \geq \gamma^{(L)} = \phi_i^2/(4l_{xy}^2 \langle x \rangle_0)[1 - (2Q - 1)(\epsilon^2 - 1)]^{-1}$ can again be expressed in terms of Q, the ratio of correlation lengths ϵ and another constant $\langle x \rangle_0$ which can be computed from the two-point correlation function. This is insofar interesting since the permeability tensor K_e is also related to γ by a bound (Ch. 23.2, Torquato, 2002), yielding a Q dependent expression for the z permeability via $K_{e,z}^{-1} \geq \gamma^{(L)}$. The relevance of the bound for the permeabilty and its dependence on Q can be immediately assessed via direct numerical simulations

A general treatment of snow microstructure

H. Löwe et al.

(Zermatten et al., 2011). We note that an isotropic version of the latter bound has been employed for the permeability of sea ice (Golden et al., 2007) which might also benefit from incorporating anisotropy, given the geometrical variability of brine pockets under temperature cycling.

All examples ubiquitously demonstrate that bounds and low-order truncations of exact expressions (i) suggest well defined and generalizable parameters and (ii) suggest functional forms between them which abandon a purely empirical treatment. Thereby cross-property relations can be formulated which are often observed for natural snow and required for a deeper understanding of the associated processes (Courville et al., 2007; Barber and Nghiem, 1999; Domine et al., 2011).

5.3 Limitations of second order bounds

Second-order treatment has indeed limitations as observed here for the less important horizontal component $k_{e,xy}$ (Fig. 5). We infer a worse performance of the bound which is no longer linearly related to simulations. Apparently, the connectivity in xy direction is more complex than in z direction. As a remedy we shall address the available, third-order improvement (Torquato and Sen, 1990) in future work. This will also help to abandon the remaining empiricism contained in the coefficients A, B in Eq. (5).

6 Conclusions

Arons and Colbeck (1995) postulated to incorporate microstructure parameters based on first-principles into parametrizations for the thermal conductivity. We have shown that second-order bounds for anisotropic materials provide such an approach which benefits from the strong, naturally occurring differences in snow anisotropy. The methodology demonstrated here for thermal conductivity can be generalized to other physical quantities for which series expansions or bounds have been derived in terms of anisotropic correlation functions. We have shown that even the strongly simplified

treatment of approximating the correlation function by an exponential form with a orientation dependent correlation length leads to a considerable reduction of scatter. This demonstrates the importance of characterizing vertical and horizontal correlation lengths of snow. The connection between the thermal conductivity and other macroscopic properties via the same parameter Q will certainly help to unify modeling efforts for various applications. The advantage for macroscopic snowpack modeling is apparent since it remains to understand the evolution of the parameter Q or $C(r)$ during metamorphism.

Supplementary material related to this article is available online at:
http://www.the-cryosphere-discuss.net/6/4673/2012/tcd-6-4673-2012-supplement.pdf.

References

Arons, E. and Colbeck, S.: Geometry of heat and mass-transfer in dry snow – a review of theory and experiment, Rev. Geophys., 33, 463–493, doi:10.1029/95RG02073, 1995. 4682, 4684

Barber, D. G. and Nghiem, S.: The role of snow on the thermal dependence of microwave backscatter over sea ice, J. Geophys. Res., 104, 789–803, 1999. 4674, 4684

Calonne, N., Flin, F., Morin, S., Lesaffre, B., du Roscoat, S. R., and Geindreau, C.: Numerical and experimental investigations of the effective thermal conductivity of snow, Geophys. Res. Lett., 38, L23501, doi:10.1029/2011GL049234, 2011. 4675, 4676, 4680

Courville, Z. R., Albert, M. R., Fahnestock, M. A., Cathles, L. M., and Shuman, C. A.: Impacts of an accumulation hiatus on the physical properties of firn at a low-accumulation polar site, J. Geophys. Res., 112, F02030, doi:10.1029/2005JF000429, 2007. 4674, 4684

Domine, F., Bock, J., Morin, S., and Giraud, G.: Linking the effective thermal conductivity of snow to its shear strength and density, J. Geophys. Res., 116, F04027, doi:10.1029/2011JF002000, 2011. 4674, 4684

Domine, F., Gallet, J.-C., Bock, J., and Morin, S.: Structure, specific surface area and thermal conductivity of the snowpack around Barrow, Alaska, J. Geophys. Res., 117, D00R14, doi:10.1029/2011JD016647, 2012. 4675, 4682

Fichefet, T., Tartinville, B., and Goosse, H.: Sensitivity of the Antarctic sea ice to the thermal conductivity of snow, Geophys. Res. Lett., 27, 401–404, doi:10.1029/1999GL002397, 2000. 4675, 4683

Fierz, C., Armstrong, R. L., Durand, Y., Etchevers, P., Greene, E., McClung, D. M., Nishimura, K., Satyawali, P. K., and Sokratov, S.: The International Classification for Seasonal Snow on the Ground, IHP-VII Technical Documents in Hydrology, 83, IACS Contribution (1), UNESCO-IHP, Paris, 2009. 4679

Flanner, M. and Zender, C.: Linking snowpack microphysics and albedo evolution, J. Geophys. Res., 111, D12208, doi:10.1029/2005JD006834, 2006. 4675

Garboczi, E. J.: Finite element and finite difference programs for computing the linear electrical and elastic properties of digital images of random material, NISTIR 6269, US Department of Commerce, 1998. 4680

Golden, K. M., Eicken, H., Heaton, A. L., Miner, J., Pringle, D. J., and Zhu, J.: Thermal evolution of permeability and microstructure in sea ice, Geophys. Res. Lett., 34, L16501, doi:10.1029/2007GL030447, 2007. 4684

Kaempfer, T., Schneebeli, M., and Sokratov, S.: A microstructural approach to model heat transfer in snow, Geophys. Res. Lett., 32, L21503, doi:10.1029/2005GL023873, 2005. 4676, 4679

Löwe, H., Spiegel, J. K., and Schneebeli, M.: Interfacial and structural relaxations of snow under isothermal conditions, J. Glaciol., 57, 499–510, 2011. 4678, 4679

Pinzer, B. and Schneebeli, M.: Breeding snow: an instrumented sample holder for simultaneous tomographic and thermal studies, Meas. Sci. Technol., 20, 095705, doi:10.1088/0957-0233/20/9/095705, 2009. 4679

Rechtsman, M. C. and Torquato, S.: Effective dielectric tensor for electromagnetic wave propagation in random media, J. Appl. Phys., 103, 084901, doi:10.1063/1.2906135, 2008. 4675, 4683

A general treatment of snow microstructure

H. Löwe et al.

Title Page

Abstract	Introduction
Conclusions	References
Tables	Figures

◀◀ ▶▶

◀ ▶

Back | Close

Full Screen / Esc

Printer-friendly Version

Interactive Discussion

Riche, F. and Schneebeli, M.: Thermal conductivity of anisotropic snow measured by three independent methods, The Cryosphere Discuss., 6, 1839–1869, doi:10.5194/tcd-6-1839-2012, 2012. 4676

Riche, F., Montagnat, M., and Schneebeli, M.: Evolution of crystal orientation in snow during temperature gradient metamorphism, J. Glaciol., 1–18, accepted, 2012. 4679

Schweizer, J., Jamieson, J., and Schneebeli, M.: Snow avalanche formation, Rev. Geophys., 41, 1016, doi:10.1029/2002RG000123, 2003. 4674

Sen, A. and Torquato, S.: Effective conductivity of anisotropic 2-phase composite media, Phys. Rev. B, 39, 4504–4515, 1989. 4675, 4677, 4683

Shertzer, R. H. and Adams, E. E.: Anisotropic thermal conductivity model for dry snow, Cold Reg. Sci. Technol., 69, 122–128, 2011. 4676

Sturm, M. and Johnson, J. B.: Thermal-conductivity measurements of depth hoar, J. Geophys. Res., 97, 2129–2139, doi:10.1029/91JB02685, 1992. 4682

Sturm, M., Holmgren, J., Konig, M., and Morris, K.: The thermal conductivity of seasonal snow, J. Glaciol., 43, 26–41, 1997. 4675, 4680

Sturm, M., Holmgren, J., and Perovich, D.: Winter snow cover on the sea ice of the Arctic Ocean at the Surface Heat Budget of the Arctic Ocean (SHEBA): temporal evolution and spatial variability, J. Geophys. Res, 107, 8047, doi:10.1029/2000JC000400, 2002a. 4682

Sturm, M., Perovich, D., and Holmgren, J.: Thermal conductivity and heat transfer through the snow on the ice of the Beaufort Sea, J. Geophys. Res., 107, 8043, doi:10.1029/2000JC000409, 2002b. 4682

Torquato, S.: Effective stiffness tensor of composite media. 1. Exact series expansions, J. Mech. Phys. Solids, 45, 1421–1448, 1997. 4675

Torquato, S.: Random Heterogeneous Materials, Springer, New York, 2002. 4675, 4680, 4682, 4683

Torquato, S. and Lado, F.: Trapping constant, thermal-conductivity, and the microstructure of suspensions of oriented spheroids, J. Chem. Phys., 94, 4453–4462, 1991. 4676, 4678, 4683

Torquato, S. and Sen, A.: Conductivity tensor of anisotropic composite media from the microstructure, J. Appl. Phys., 67, 1145–1155, 1990. 4675, 4676, 4677, 4678, 4684

Vallese, F. and Kong, J.: Correlation-function studies for snow and ice, J. Appl. Phys., 52, 4921–4925, 1981. 4678

Title Page

Abstract | Introduction

Conclusions | References

Tables | Figures

|◀ | ▶|

◀ | ▶

Back | Close

Full Screen / Esc

Printer-friendly Version

Interactive Discussion

Wiesmann, A., Matzler, C., and Weise, T.: Radiometric and structural measurements of snow samples, Radio Sci., 33, 273–289, 1998. 4678

Zermatten, E., Haussener, S., Schneebeli, M., and Steinfeld, A.: Tomography-based determination of permeability and Dupuit–Forchheimer coefficient of characteristic snow samples, J. Glaciol., 57, 811–816, 2011. 4684

A general treatment of snow microstructure

H. Löwe et al.

Title Page

Abstract | Introduction

Conclusions | References

Tables | Figures

|◄ | ►|

◄ | ►

Back | Close

Full Screen / Esc

Printer-friendly Version

Interactive Discussion
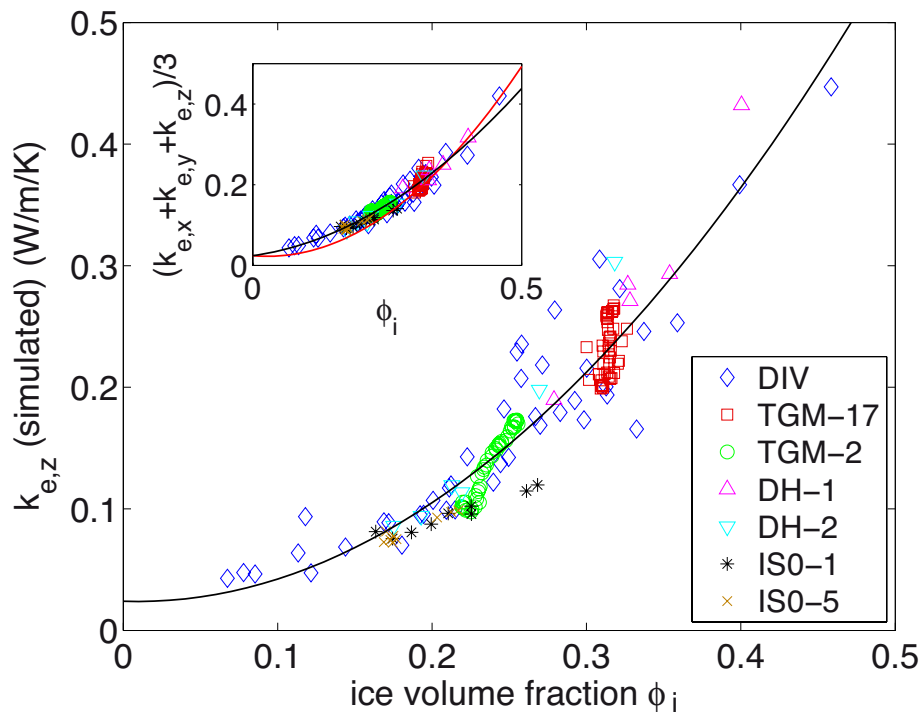
Fig. 1. Simulated vertical conductivity $k_{e,z}$ as a function of volume fraction and quadratic fit (black line). Inset: directionally averaged conductivity. Black and red line: quadratic fits, details in the text.
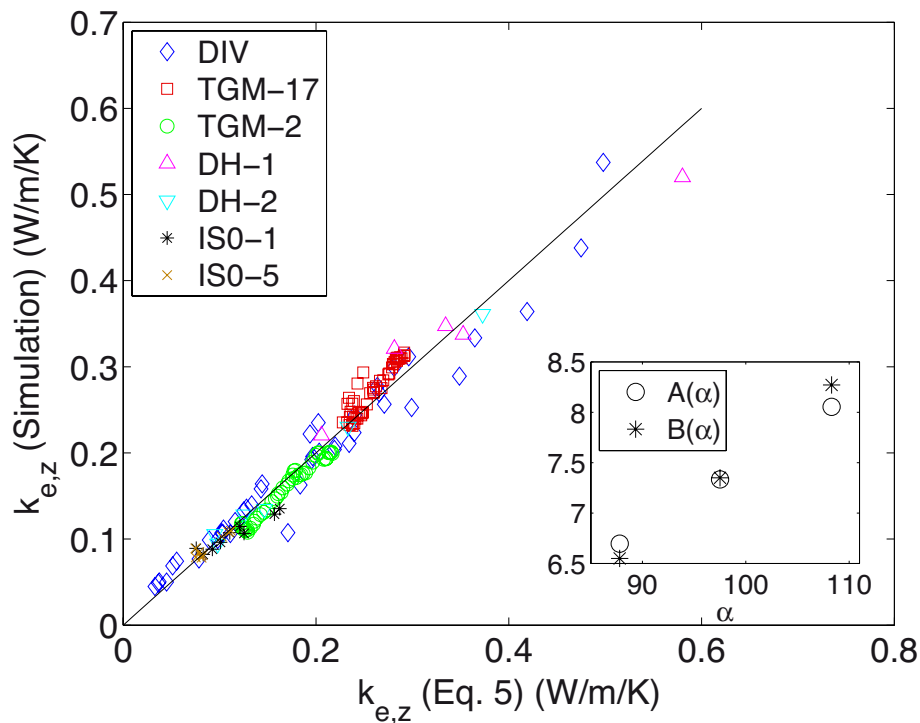
Fig. 2. Comparison of the simulated vertical conductivity to Eq. (5) suggested by the bound. Deviations from the $1:1$ correspondence (black line) yield $R^2 = 0.96$. The inset shows the coefficients in Eq. (5) obtained for different α.

A general treatment of snow microstructure

H. Löwe et al.

Title Page

Abstract	Introduction
Conclusions	References
Tables	Figures

|◀ | ▶|

◀ | ▶

Back | Close

Full Screen / Esc

Printer-friendly Version

Interactive Discussion
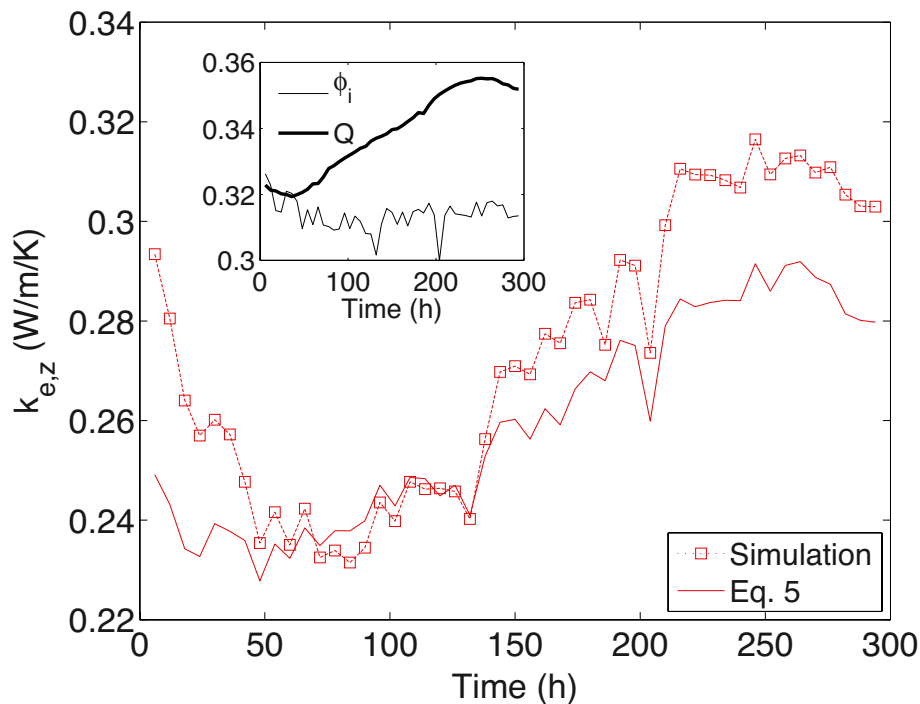
Fig. 3. Comparison of the model Eq. (5) with simulations for one metamorphism time series (TGM-17). The inset shows the evolution of the parameters Q, ϕ_i.

Full Screen / Esc

Printer-friendly Version

Interactive Discussion
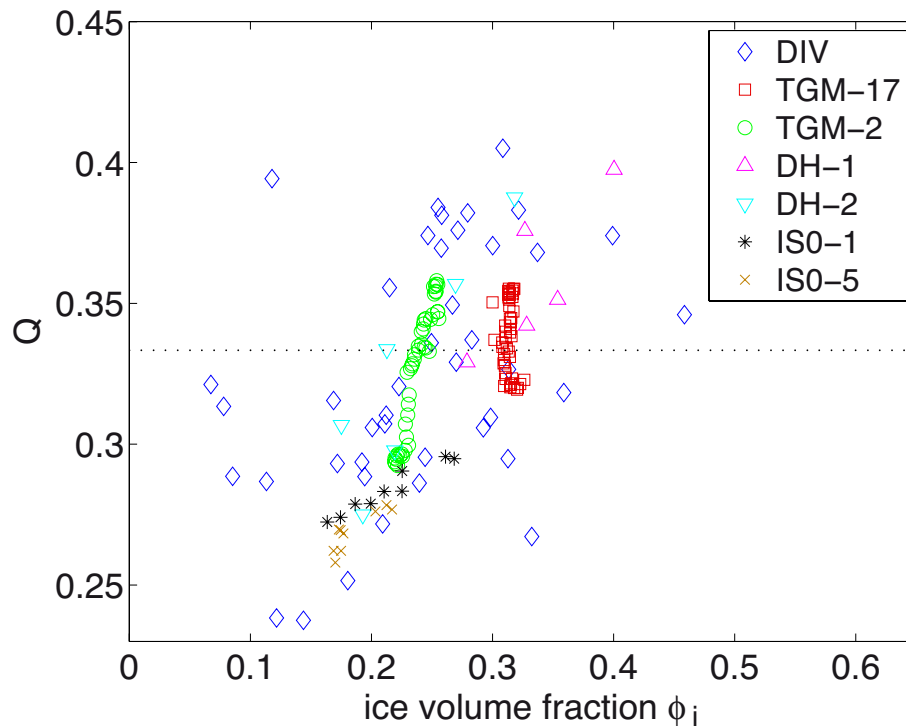
Fig. 4. Distribution of microstructural parameters in the (ϕ_i, Q) plane. The dashed line $Q = 1/3$ indicates isotropy.

Fig. 5. Comparison of the simulated horizontal conductivity to the prediction of the bound.

Title Page

Abstract | Introduction

Conclusions | References

Tables | Figures

|◄ | ►|

◄ | ►

Back | Close

Full Screen / Esc

Printer-friendly Version

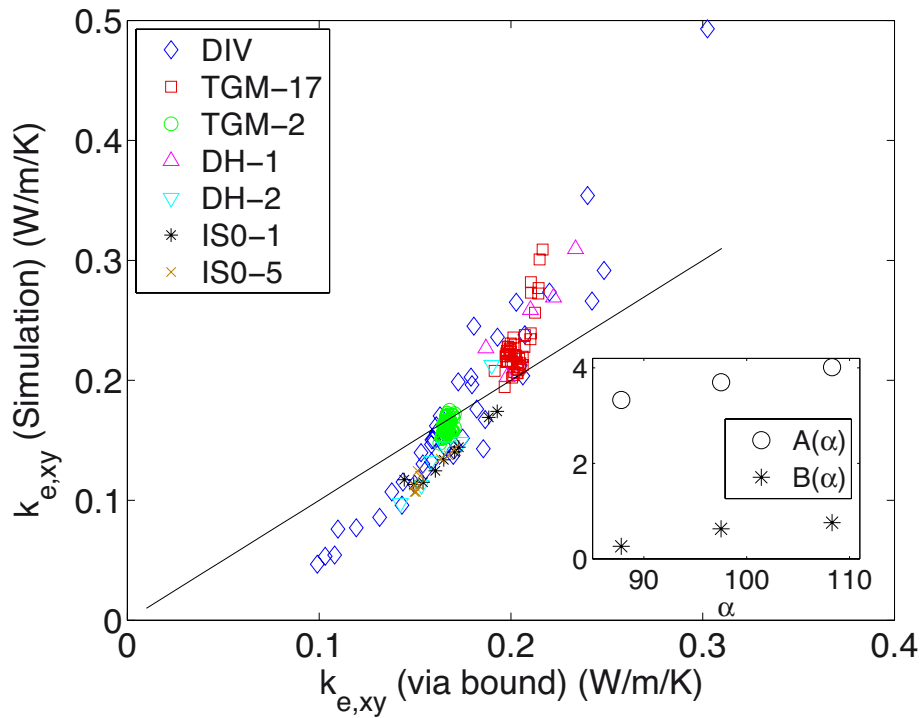Interactive Discussion